Kinematic Redundancy Analysis during Goal-Directed Motion for Trajectory Planning of an Upper-Limb Exoskeleton Robot*

Chen Wang[1,2], Liang Peng[1], Zeng-Guang Hou[1,3], Jingyue Li[4], Lincong Luo[1,2], Sheng Chen[1,2], and Weiqun Wang[1]

***Abstract*— The kinematic redundancy of human arm imposes challenges on joint space trajectory planning for upper-limb rehabilitation robot. This paper aims to investigate normal motion patterns in reaching and reach-to-grasp movements, and obtain the unique solution in joint space for a five-DOF exoskeleton. Firstly, a six-camera optical motion tracking system was used to capture participants' arm motion during goal-directed reaching or reach-to-grasp movements. Secondly, statistical analysis was executed to explore the characteristics of swivel angle, which revealed that the swivel angle can be approximated to the mean value $(155^\circ \pm 5^\circ)$ in resolving the arm redundancy problem. Thirdly, combined with the minimum-jerk trajectory of end-effector, the generated joint trajectory complied well with the joint trajectory captured in healthy humans. Consequently, the obtained results facilitate a new way for three-dimensional trajectory planning of the exoskeleton robot. Further, adaptive assist-as-needed control of the exoskeleton robot can be implemented based on the optimal reference trajectory, with aims to provide assistance according to the patient's performance, and in turn promote neural plasticity.**

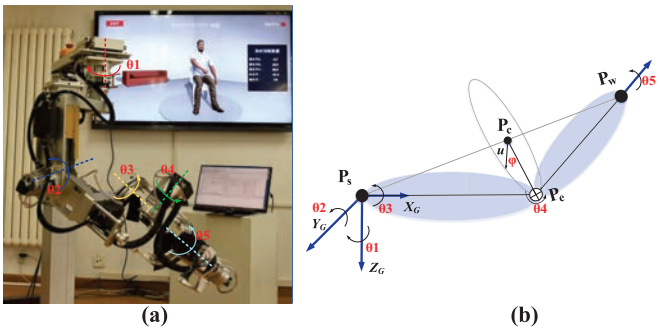

(a) (b)

Fig. 1: (a) The five-DOF upper-limb rehabilitation robot exhibits a kinematic redundancy similar to human arm. Axis 1-3 depict the shoulder internal-external rotation, flexion-extension, adduction-abduction, respectively. Axis 4 represents the elbow flexion-extension. Axis 5 represent the wrist supination-pronation. (b) Kinematic model of the human arm.

I. INTRODUCTION

The Global Burden of Disease (GBD) showed that the absolute numbers of post-stroke patients who died from their stroke is increasing [1]. According to the statistics from WHO (World Health Organization), stroke has become the main cause of non-traumatic disability and the second leading cause of death [2]. Long-term physical therapy and occupational therapy are important for the recovery of motor impairment as a consequence of promoting neural plasticity. Compared with conventional rehabilitation training accomplished manually by therapists, robot-assisted rehabilitation is believed to be more promising for its advantages in good repeatability, quantitative assessment, low cost, etc [3].

The effectiveness of robot-aided therapy relies heavily on control strategies, and for the implementation of both passive and active training, reference trajectory is required to be generated beforehand. Especially for exoskeleton-type robot as shown in Fig. 1(a) developed by us, each joint should be controlled on the basis of normal motion patterns and the patient motion intention [4]. More concretely, based on the motion pattern of end-effector in workspace, the desired trajectory in joint space can be derived from inverse kinematics. However, as the kinematic redundancy of the upper-limb exoskeleton robot is identical to the human upper limb, it's difficult to obtain a unique solution for inverse kinematics, which becomes a major obstacle in reproducing the therapists corrections during the rehabilitation training.

The symptoms often observed on post-stroke patients are that they cannot solve the kinematic redundancy properly and exhibit pathological synergies between shoulder and elbow joints [5]. In order to help patients reacquire the appropriate redundancy resolution and recover the impairment of inter-joint coordination, rather than only providing end-point rehabilitation training [6], the upper-limb exoskeleton robot should focus on inhibiting the abnormal inter-joint synchronization of arm movements. Therefore, this study aims to explore the redundancy resolution adopted by healthy subjects, which is critical to three-dimensional trajectory planning of the exoskeleton robot.

The kinematic redundancy of human arm enables infinite arm postures to complete the task in a three-dimensional workspace, which can be resolved by calculating a unique swivel angle. Prior literature utilized the performance criteria

*This work was supported in part by National Natural Science Foundation of China (Grant #61603386, U1613228, 61720106012, 61533016, 61421004) and Beijing Natural Science Foundation (Grant L172050), and also supported by the Strategic Priority Research Program of Chinese Academy of Science (Grant No.XDB32040000).

[1]State Key Laboratory of Management and Control for Complex Systems, Institute of Automation, Chinese Academy of Sciences, Beijing 100190, China; Emails:{wangchen2016, liang.peng, zengguang.hou, luolincong2014, chensheng2016, weiqun.wang}@ia.ac.cn

[2]University of Chinese Academy of Sciences, Beijing 100049, China;

[3]CAS Center for Excellence in Brain Science and Intelligence Technology, Beijing 100190, China.

[4]China Rehabilitation Research Center, Beijing Bo'ai Hospital, Beijing 100068, China; Email:lijingyue87@126.com

including energy consumption [7], task accuracy [8], and smoothness of movement [9] to select the swivel angle. However, such methods have two main limitations in implementation: firstly, the existence of ill-posed inverse problems may lead to numerical instability; besides, the high level computation complexity makes it difficult to realize real-time control of the rehabilitation robot.

The overarching goal of this study is to explore the redundancy resolution in healthy humans, which provides a quantitative basis for three-dimensional trajectory planning of the upper-limb exoskeleton robot. In this paper, we focus on the reaching and reach-to-grasp movements, which are the most commonly used tasks in upper-limb rehabilitation training, and designed an experiment platform that allows for different positions and directions goal-directed movements. Swivel angles were calculated from the motion data captured by an optical motion tracking system, and statistical analysis was executed. Furthermore, combined with the minimum-jerk trajectory approximation of the end-effector, the results of joint trajectory planning were coincident well with the joint trajectories captured during the experiment.

In the remaining parts of this study: Section II describes a five-DOF kinematic model compatible with the exoskeleton robot, and introduces the kinematic redundancy of human arm. Section III details the experimental apparatus and the design of two experiments. Then the data processing and experimental results are presented in Section IV, and Section V concludes the paper.

II. MODELING OF HUMAN ARM

A. Kinematic Model

The human arm can be simplified as two rigid links articulated by three joints: shoulder joint, elbow joint and wrist joint (see Fig. 1(b)). There are seven DOFs of the entire arm: shoulder spherical joint three DOFs, elbow revolute joint one DOF, and wrist spherical joint three DOFs. For the upper-limb exoskeleton robot, shoulder joint and elbow joint are identical to the human arm, while wrist joint is confined to supination-pronation. Accordingly, a five-DOF human arm model is described in this section, which is compatible with the exoskeleton robot.

Placing the origin of the coordinate system at the shoulder, and defining $A_i\,(i = 1 \cdots 5)$ as the state transition matrix, the value of A_i can be expressed in terms of the joint variable θ_i:

$$A_1 = R(z,\theta_1) = \begin{bmatrix} c1 & -s1 & 0 & 0 \\ s1 & c1 & 0 & 0 \\ 0 & 0 & 1 & 0 \\ 0 & 0 & 0 & 1 \end{bmatrix}$$

$$A_2 = R(y,\theta_2) = \begin{bmatrix} c2 & 0 & -s2 & 0 \\ 0 & 1 & 0 & 0 \\ s2 & 0 & c2 & 0 \\ 0 & 0 & 0 & 1 \end{bmatrix}$$

$$A_3 = R(x,\theta_3)T(l_1,0,0) = \begin{bmatrix} 1 & 0 & 0 & l_1 \\ 0 & c3 & s3 & 0 \\ 0 & -s3 & c3 & 0 \\ 0 & 0 & 0 & 1 \end{bmatrix}$$

$$A_4 = R(y,\theta_4)T(l_2,0,0) = \begin{bmatrix} c4 & 0 & s4 & c4l_2 \\ 0 & 1 & 0 & 0 \\ -s4 & 0 & c4 & -s4l_2 \\ 0 & 0 & 0 & 1 \end{bmatrix}$$

$$A_5 = R(x,\theta_5) = \begin{bmatrix} 1 & 0 & 0 & 0 \\ 0 & c5 & s5 & 0 \\ 0 & -s5 & c5 & 0 \\ 0 & 0 & 0 & 1 \end{bmatrix}$$

where s_i and c_i refer to $\cos(\theta_i)$ and $\sin(\theta_i)$, respectively; l_1 and l_2 represent the length of the upper arm and lower arm.

For the desired position and pose of the wrist joint, inverse kinematics can be solved by finding angles $\theta_i\,(i = 1 \cdots 7)$ compatible with the following relationship:

$$A_1A_2A_3A_4A_5A_6A_7 = A_{wrist}. \tag{1}$$

where A_6 and A_7 are identity matrices for our robot.

Assuming that the elbow position is known, the unique values of θ_1 and θ_2 are given as:

$$\begin{matrix} \theta_1 = \arctan 2(y_e, x_e) \\ \theta_2 = \arcsin(z_e/l_1) \end{matrix}. \tag{2}$$

Once the wrist position that depends on the first four joints is known, the matrix equation can be simplified and then yield the unique solution for θ_3:

$$\theta_3 = \arctan 2(c1y_w - s1x_w, c2z_w - c1s2x_w - s1s2y_w). \tag{3}$$

Additionally, the elbow angle θ_4 is determined by the distance between the wrist position P_w and the shoulder position P_s:

$$\theta_4 = \pi - \arccos \frac{l_1^2 + l_2^2 - \|P_w - P_s\|^2}{2l_1l_2}. \tag{4}$$

To solve the wrist rotation angle θ_5, (1) can be rearranged into the following form:

$$A_5A_6A_7 = (A_1A_2A_3A_4)^{-1}A_{wrist}, \tag{5}$$

which yields the possible solution:

$$\theta_5 = \arctan 2(r23, r33), \tag{6}$$

where $\begin{bmatrix} r11 & r12 & r13 \\ r21 & r22 & r23 \\ r31 & r32 & r33 \end{bmatrix} = (A_1A_2A_3A_4)^{-1}A_{wrist}.$

B. Redundant Degree of Freedom: Swivel Angle

Assuming that the position of elbow joint and wrist joint are known, the solution for inverse kinematics can be uniquely determined by solving the equation (2)-(6). However, in most ADL (activities of daily living) training, only the target position i.e., the desired wrist position is known beforehand, while the elbow position is not fully specified.

Given a fixed position of wrist in three-dimensional workspace, the plane determined by the position of shoulder, elbow and wrist still can swivel about an axis from the shoulder to the wrist. The kinematic redundancy reflects in the indefinite position of the elbow, which can be represented mathematically by a swivel angle ϕ (see Fig. 1(b)).

Placing a coordinate system at the center of the elbow circle P_c which is orthogonal to the vector in direction of the shoulder to the wrist, the coordinate basis is defined as:

$$\begin{aligned} \overrightarrow{n} &= \frac{P_w - P_s}{\|P_w - P_s\|} \\ \overrightarrow{u} &= \frac{(z \cdot \overrightarrow{n})\overrightarrow{n} - z}{\|(z \cdot \overrightarrow{n})\overrightarrow{n} - z\|} \\ \overrightarrow{v} &= \overrightarrow{n} \times \overrightarrow{u}, \end{aligned} \tag{7}$$

where P_w and P_s are respectively the positions of the wrist and shoulder, and the unit vector $\overrightarrow{u}$ can be considered as the projection of the z axis onto the plane containing the elbow circle.

The swivel angle ϕ, determining the elbow position in the circle, can be defined as the angle between $\overrightarrow{u}$ and $\overrightarrow{P_e - P_c}$. Once the value of ϕ is known, the elbow position can be calculated by the following trigonometry [10]:

$$\begin{aligned} \cos(\sigma) &= \frac{l_1^2 + \|P_w - P_s\|^2 - l_2^2}{2 l_1 \|P_w - P_s\|} \\ P_c &= P_s + l_1 \cos(\sigma) \cdot \overrightarrow{n} \\ d &= l_1 \sin(\sigma) \\ P_e &= d\,[\cos(\phi) \cdot \overrightarrow{u} + \sin(\phi) \cdot \overrightarrow{v}] + P_c, \end{aligned} \tag{8}$$

where d represents the radius of the elbow circle.

Consequently, the human arm redundancy can be resolved by selecting the value of swivel angle, and the following sections will investigate the characteristics of swivel angle and joint synergies in spatial reaching and reach-to-grasp tasks that performed by healthy individuals.

III. EXPERIMENTAL METHODS

A. Participants

Six right-handed healthy subjects (two males, four females) participated in the experiments, and they were in the 27-34 age range, with heights ranging from 167 to 187 cm. All participants were able-bodied, and had normal or corrected-to-normal vision. The experimental protocols involving human subjects described in this paper were approved by the Institutional Review Board.

B. Experimental Apparatus

An experimental platform with nine targets in front of the participant was designed, and in order to elicit reach-to-grasp movements of different directions, we used the cylindrical iron box as handle which was attracted by magnets on the plate, and could be rotated to a fixed orientation (see Fig. 2). The distance between the chair and the workspace was adjusted according to 90% of the participant's arm length, and the height of the experimental platform was individually positioned to guarantee that the central target was aligned with the participant's right shoulder.

To record the kinematic data during the movements, we used a six-camera optical motion tracking system (Qualisys AB, Gothenburg, Sweden), which can capture the motion of Qualisys super-spherical markers. Sixteen spherical markers were attached to participants' body at anatomical positions, and the three-dimensional coordinates of markers were sampled at 200Hz.

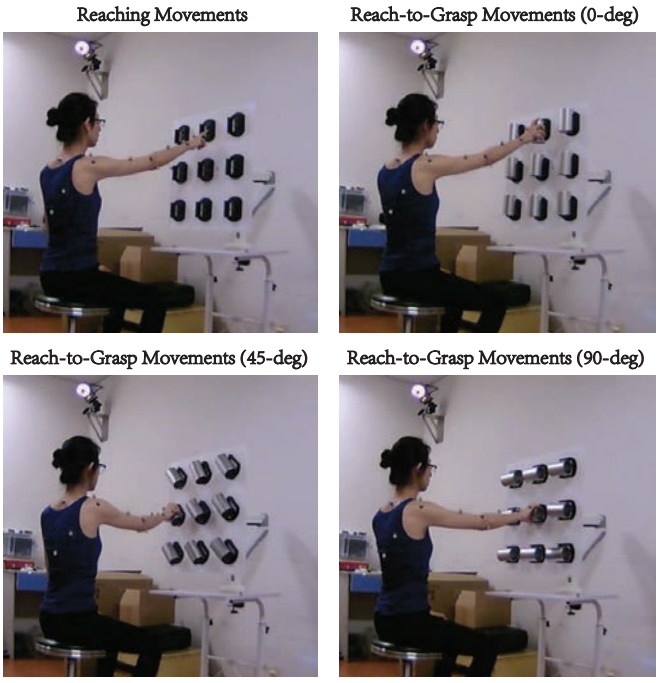

Fig. 2: Experimental set-up: illustration of the reaching movements and the reach-to-grasp movements, where the participant was instructed to point or grasp the specified target.

C. Experimental Protocols

Two types of experimental tasks were derived from the upper-limb rehabilitation training, including reaching tasks and reach-to-grasp tasks. In all experiments, participants sat up straight on a stool. To elicit natural and unrestrained movements, we instructed participants to move at a relatively high speed. Importantly, participants were encouraged to accomplish experimental tasks by moving only the right arm, with the aim to minimize the displacement of the shoulder joint.

1) Design of Experiment 1 (Reaching Movements): In this experiment, six participants were instructed to make reaching movements with their right arms toward each of the nine targets. Each participant conducted nine sessions, each consisting of six successive reaching movements. In the initial posture, the participant rested his/her right hand on the center of the tabletop which was marked as the starting position. After the starting signal, the participant used his/her index finger to point the instructed target grossly, and the target number that the reaching movements ended at was informed before trials.

2) Design of Experiment 2 (Reach-to-Grasp Movements): This experiment aimed to detect the effect of wrist orientation on the value of swivel angle. Similar to Experiment 1, Experiment 2 also contained nine sessions, but in each session, there were three subsessions which depended on the orientation of handles (0-deg, 45-deg, 90-deg in relation to the direction of gravity). Within each subsession, the participant was asked to move the hand from the starting position

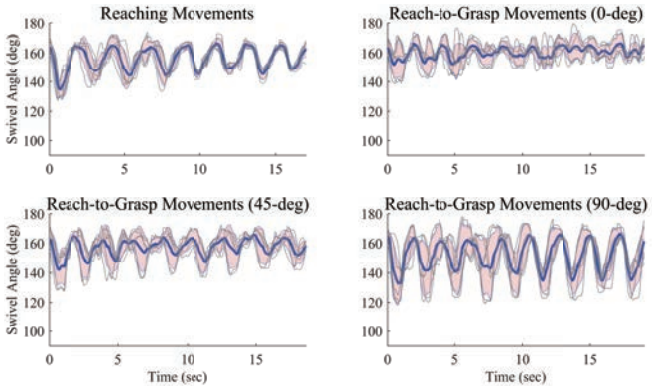

Fig. 3: Time-series swivel angles of all participants in reaching movements and reach-to-grasp movements (0-deg, 45-deg, 90-deg). Gray lines indicate the evolutions of the swivel angle in individual participant's average motion. Thick blue lines indicate the averages of six participants across all trials. Shade zone indicate the across-participants and across-trials standard deviation.

which was the same as in Experiment 1 to the instructed target in a specific direction. After the starting signal was given, the participant performed reaching movements and grasped the target in a comfortable posture, and there were two successful trial in each subsession.

D. Data Processing

The motions of markers were transformed from sequential frames to three-dimensional coordinates by Visual3D software (C-Motion, Rockville, Canada). For the kinematic analysis of Experiment 1 and Experiment 2, joint angles were calculated on the basis of the kinematic model described in Section II-A, which contained shoulder internal-external rotation, shoulder flexion-extension, shoulder adduction-abduction, elbow flexion-extension, wrist supination-pronation, and swivel angle. These kinematic data was normalized by resampling, in order to select 200 points evenly spaced between the movement onset and termination, and then the average trials for each participant were obtained based on the repetitions of the same experimental task.

IV. RESULTS

A. Swivel Angle and Redundancy Resolution

Based on the swivel angle calculated from the captured motion data, we first studied the regularity of swivel angle, which can provide the background for resolving the kinematic redundancy. Figure 3 presents the time-series swivel angles of all participants, for the four different experimental tasks. Despite there were small variations in the magnitude, the swivel angle profiles were essentially consistent and had the similar mean-angle profiles. For statistical analysis, we summarized the mean value and standard deviation of swivel angles across all participants for the four different goal-directed movements in Table I.

It can be seen that the variation of swivel angle was small and ranged from 138.73° to 165.69° over all experiments.

TABLE I: Mean value and standard deviation of swivel angles for Experiment 1 and Experiment 2.

Task	Reaching	Reach-to-Grasp		
		0-deg	45-deg	90-deg
Mean	156.08°	160.52°	157.35°	155.49°
Std	5.08°	5.98°	7.04°	6.57°

Therefore, the kinematic redundancy of human arm can be resolved by fixing the value of swivel angle. Besides the redundancy resolution that yields the unique solutions for joint variables, the three-dimensional trajectory planning also concentrates on the motion pattern of end-effector. Therefore, we postulated that the spatial trajectory of end-effector can be generated based on the minimum-jerk model [11], and the minimum-jerk trajectory from (x_i, y_i, z_i) to (x_d, y_d, z_d) were calculated:

$$\begin{aligned} x(t) &= x_i + (x_d - x_i)\left(10\tau^3 - 15\tau^4 + 6\tau^5\right) \\ y(t) &= y_i + (y_d - y_i)\left(10\tau^3 - 15\tau^4 + 6\tau^5\right) \\ z(t) &= z_i + (z_d - z_i)\left(10\tau^3 - 15\tau^4 + 6\tau^5\right) \end{aligned} \quad , \qquad (9)$$

where $\tau = t/t_d$, and t_d is the total time of the goal-directed movements; (x_i, y_i, z_i) and (x_d, y_d, z_d) represent the coordinates of initial point and end point, respectively.

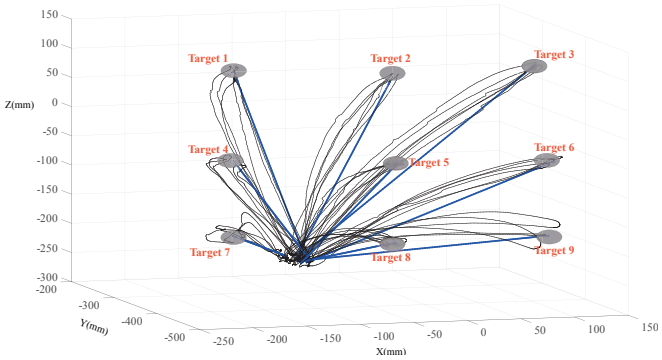

Fig. 4: Wrist trajectories of a representative participant, captured in the reaching movements. Grey lines indicate three-dimensional trajectories toward the nine different targets. Thick blue lines indicate standard minimum-jerk profiles.

Figure 4 shows the representative spatial trajectories of wrist joint for nine targets in Experiment 1, as well as nine standard minimum-jerk trajectories. As participants were instructed to make goal-oriented reaching movements with right hands, the real trajectories were slightly curved rightward. Consequently, the small deviations between the real trajectories and the generated minimum-jerk profiles were observed in Fig. 4, which supported the hypothesis.

Further, considering that the shoulder joint angles (θ_1, θ_2, θ_3) and wrist joint angle (θ_4) were determined by the elbow position for a particular reaching or grasping task, we calculated the four joint angles on the basis of a constant swivel angle and a minimum-jerk trajectory, in order to examine whether the swivel angle can be approximated to the

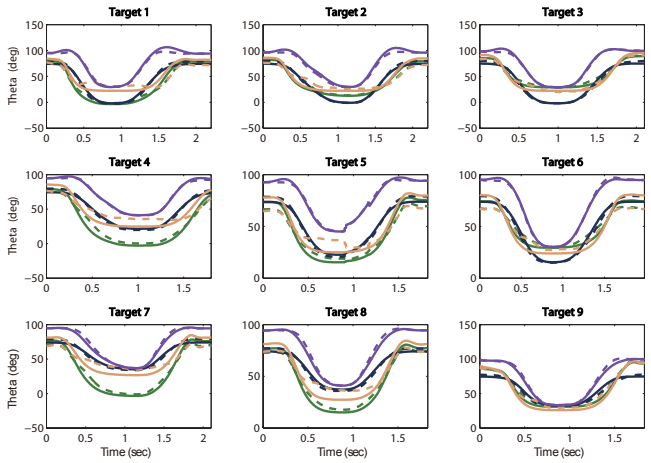

Fig. 5: Joint angles comparison from a representative participant. Solid lines represent the estimated joint angles for the reaching movements toward the nine targets. Dotted lines represent the corresponding joint angles measured in goal-oriented reaching movements. The dark green, navy blue, yellow and purple lines represent θ_1, θ_2, θ_3 and θ_4 respectively.

mean value during the point-to-point movements and verify the hypothesis that arm motion in three-dimensional space complies well with the minimum-jerk principle.

TABLE II: RMS of the estimation error, for the four types of point-to-point movements.

	Reaching	Reach-to-Grasp		
		0-deg	45-deg	90-deg
Participant 1	4.72°	3.88°	4.70°	6.31°
Participant 2	5.97°	4.61°	5.76°	7.52°
Participant 3	5.55°	4.97°	6.78°	8.42°
Participant 4	4.95°	3.74°	4.38°	6.27°
Participant 5	5.27°	4.68°	4.62°	6.50°
Participant 6	4.63°	3.92°	5.30°	7.11°

Figure 5 displays the comparison between estimated joint angles and measured joint angles obtained form a representative participant in Experiment 1. Table II summarizes the average RMS errors of estimated $\theta_1 \sim \theta_4$, for the four types of goal-directed movements. It can be concluded that the estimated joint angles of shoulder and wrist were coincident well with the measured joint angles for reaching or reach-to-grasp movements toward each of the nine targets. Therefore, two conclusions drawn from these results were worthy of note:

- In reaching movements and reach-to-grasp movements, the swivel angle maintained a relatively constant value, which can be approximated to the mean value in resolving the kinematic redundancy of human arm.
- The movements of end-effector were proven to be successfully substituted by a normal minimum-jerk trajectory, and by combining with the regularity of swivel angle, the corresponding joint angle trajectories were able to be calculated through inverse kinematics.

V. CONCLUSIONS

In this study, we investigated the redundancy resolution adopted by healthy humans and provide a basis for three-dimensional trajectory planning of our exoskeleton robot. Experiments of reaching and reach-to-grasp tasks demonstrated that the swivel angle maintained a relatively constant value for different targets and can be approximated to the mean value in resolving the arm redundancy problem. Integrated with the minimum-jerk trajectory of end-effector, the reference trajectories of all joints were obtained and the RMS values of fitting errors were relatively small. The future work will concentrate on the implementation of adaptive assist-as-needed control around the reference trajectory, which is supposed to be beneficial to more effective human-robot interaction and fastest possible recovery.

REFERENCES

[1] V. L. Feigin, R. V. Krishnamurthi, P. Parmar, B. Norrving, G. A. Mensah, D. A. Bennett, S. Barker-Collo, A. E. Moran, R. L. Sacco, T. Truelsen *et al.*, "Update on the global burden of ischemic and hemorrhagic stroke in 1990-2013: the gbd 2013 study," *Neuroepidemiology*, vol. 45, no. 3, pp. 161–176, 2015.

[2] L. Peng, Z.-G. Hou, L. Peng, L. Luo, and W. Wang, "Robot assisted rehabilitation of the arm after stroke: prototype design and clinical evaluation," *Science China Information Sciences*, vol. 60, no. 7, p. 073201, 2017.

[3] A. C. Lo, P. D. Guarino, L. G. Richards, J. K. Haselkorn, G. F. Wittenberg, D. G. Federman, R. J. Ringer, T. H. Wagner, H. I. Krebs, B. T. Volpe *et al.*, "Robot-assisted therapy for long-term upper-limb impairment after stroke," *New England Journal of Medicine*, vol. 362, no. 19, pp. 1772–1783, 2010.

[4] T. Nef, M. Guidali, and R. Riener, "Armin iii–arm therapy exoskeleton with an ergonomic shoulder actuation," *Applied Bionics and Biomechanics*, vol. 6, no. 2, pp. 127–142, 2009.

[5] N. Jarrassé, T. Proietti, V. Crocher, J. Robertson, A. Sahbani, G. Morel, and A. Roby-Brami, "Robotic exoskeletons: a perspective for the rehabilitation of arm coordination in stroke patients," *Frontiers in human neuroscience*, vol. 8, p. 947, 2014.

[6] E. T. Wolbrecht, V. Chan, D. J. Reinkensmeyer, and J. E. Bobrow, "Optimizing compliant, model-based robotic assistance to promote neurorehabilitation," *IEEE Transactions on Neural Systems and Rehabilitation Engineering*, vol. 16, no. 3, pp. 286–297, 2008.

[7] T. Kang, J. He, and S. I. H. Tillery, "Determining natural arm configuration along a reaching trajectory," *Experimental Brain Research*, vol. 167, no. 3, pp. 352–361, 2005.

[8] C. M. Harris and D. M. Wolpert, "Signal-dependent noise determines motor planning," *Nature*, vol. 394, no. 6695, p. 780, 1998.

[9] T. Flash and N. Hogan, "The coordination of arm movements: an experimentally confirmed mathematical model," *Journal of neuroscience*, vol. 5, no. 7, pp. 1688–1703, 1985.

[10] D. Tolani and N. I. Badler, "Real-time inverse kinematics of the human arm," *Presence: Teleoperators & Virtual Environments*, vol. 5, no. 4, pp. 393–401, 1996.

[11] R. Shadmehr, S. P. Wise *et al.*, *The computational neurobiology of reaching and pointing: a foundation for motor learning*. MIT press, 2005.